IMAGE FUSION OF UNREGISTERED COLOUR DIGITAL PATHOLOGY IMAGES

Wael Saafin[*1], *Gerald Schaefer* [1], *Miguel Vega*[2], *Rafael Molina*[3], *Aggelos Katsagelos*[4]

[1] Dept. of Computer Science, Loughborough University, Loughborough, United Kingdom.
[2] Dept. of Languages and Information Systems, University of Granada, Granada, Spain.
[3] Dept. of Computer Science and Artificial Intelligence, University of Granada, Granada, Spain.
[4] Dept. of Electrical Engineering and Computer Science, Northwestern University, Evanston, USA.
waelsaafin@hotmail.com, gerald.schaefer@ieee.org, mvega@ugr.es,
rms@decsai.ugr.es, aggk@eecs.northwestern.edu

ABSTRACT

Visual investigation of colour digital pathology (DP) images, which is better performed on improved captured images, has enormous interest. This work fuses multiple unregistered DP images to merge the information provided by each image. We propose a robust reconstruction approach that iteratively alternates between fused colour image recovery and registration parameter estimation. The image is found by optimising a function which combines fidelity to the data with a regulariser of the sought after image. We perform an accurate estimation of registration parameters which is crucial to obtain good recovered images for better visualisation and improved diagnosis. Using the proposed iterative approach, images are efficiently estimated at high convergence rates. Experiments were performed on simulated images and on real DP images as well, and the results have shown excellent quality of the estimated image.

Index Terms— Medical imaging, digital pathology, whole slide images, image fusion, image reconstruction,.

1. INTRODUCTION

Digital pathology (DP) imaging starts with tissue sample preparation, then scans the sample under a microscope using a virtual slide scanner, and finally the scanned view is sampled using a digital camera. The resulting digital whole slide image (WSI) represents high resolution digital images of complete glass histopathology or cytopathology slides, usually in standard red-green-blue (RGB) colour format. In the RGB representation, every pixel in the image plane is represented by three values corresponding to the red, green and blue components, which together constitute the overall colour of a pixel. A three channel RGB camera, typically a charge coupled device (CCD) camera, allows for colour detection and processing of the WSI. The resulting WSI usually is very large and a virtual slide viewer is required to investigate the tissue on display. WSI is useful for quality assurance, image analysis, and tracking how an image was viewed, and ultimately to aid in diagnosis [Weinstein et al., 2009, Glatz-Krieger et al., 2006].

DP studies the WSI instead of the sample fixed on a glass slide, and it is therefore recommended for histopathology and cytology samples. DP analysis techniques were proposed to detect diseases, determine its grading and type, cell structure, function, and chemistry [Hamilton et al., 2014, Irshad et al., 2014, Kothari et al., 2013, Veta et al., 2014, Saafin and Schaefer, 2017].

Any analysis of DP images should appropriately exploit the colour or spectral information residing in the obtained data. This is important to come up with stains and/or antibodies used to highlight microscopic components of the tissue under study, which selectively colour components in a tissue to enhance its visualisation.

∗ Corresponding Author.

Haematoxylin-eosin (H&E) stainings are routinely used to stain cell nuclei in blue/purple and cytoplasm and connective tissue in pink. Similarly; immunohistochemistry (IHC) highlights specific antigens in the tissue by injecting antibodies in the slide [Irshad et al., 2014].

In some cases a pathologist needs to visualise several stains at the same time and relate them to each other. This is a difficult task unless multiple slides can be merged in one image. This enables the pathologist to definitely locate different components in the image. Staining a sample with multiple stains can be done by either staining the slide with the required stains simultaneously, or by staining slides sequentially one stain at a time. The former approach necessitates unmixing techniques to separate stains that expectedly can result in new mixed colours when two or more stains add up at same location. Following the sequential approach each slide will have one stain, but will have multiple images that all are required to be included in analysis.

Medical image fusion combines two or more images to allow improved visualisation of abnormalities, ascertain differences in tissue, and to help in diagnosis. It has been applied to combine images of both the same and different modalities. A single modal fusion of medical images has been applied to ultrasound images to improve acquisition and visualisation of fetal heart [Gooding et al., 2010]. Although not applied to DP images, [Kobayashi et al., 2007] employed five quantum dots of similar sizes but different emission colours and captured observations in a sequential manner, one colour at a time. Then the observations were merged in one multicolour image to allow simultaneous visualisation and to predict the route of cancer metastasis into the lymph nodes. Medical image fusion has been applied also on different image modalities, where two images of different types are fused. The type might be magnetic resonance imaging (MRI), computed tomography (CT), position emission tomography (PET), and single photon emission computed tomography (SPECT) [Townsend and Beyer, 2002, Chajari et al., 2002, Sonn et al., 2014, Holupka et al., 1998]. Medical image fusion is a challenging problem due to the nature of the medical image modality [James and Dasarathy, 2014]. Image fusion can be classified into pixel-level and transform-based fusions. This work belongs to the pixel, or spatial level techniques [Galande and Patil, 2013].

To fuse two or more images the warping parameters should be either known or estimated for all observations. The warping parameters are those which can geometrically transform an image to fit with another, that is to realign images together. This work assumes the realistic case where the parameters are unknown and the images are unregistered then estimates them.

Image registration of DP images, which offers realignment of observations without fusing it, was addressed in [Déniz et al., 2015, Wang et al., 2014]. In [Déniz et al., 2015] sequentially stained images were used, where an observation is aligned to another. In [Wang et al., 2014] deformation problems like morphological distortions was included in a robust image registration method to align microscopic images. The output image in the two works does not offer visualisation or merging the information from the input observations. Our work shows simultaneously the visual information from all input observations into the output image making it possible to automatically or visually analyse the output image instead of the original observations. Moreover, the proposed method is applicable to two or more input images.

In this paper, we present an algorithm to fuse multiple colour DP images. This offers simultaneous visualisation of multiple images which can aid pathologists when investigating a WSI. To the best of our knowledge there is no published work addressing this exact approach of DP fusion. The proposed image reconstruction technique assumes unregistered input DP images, then aims to calculate one output image and hence estimates the fused image and registration parameters in a robust approach.

The rest of this paper is organised as follows: the problem is modelled and formulated in Section 2, while the proposed approach is presented in Section 3. Experimental results are presented in Section 4, then conclusions are stated in Section 5.

2. MODEL

Let us assume that we have access to a set of Q RGB colour images of the form

$$\mathbf{y}_{cq} = \mathbf{C}(\mathbf{s}_q)\mathbf{x}_c\,, \text{ for } q = 1, \ldots, Q, \tag{1}$$

where $c \in \{R, G, B\}$ denotes one of the three channels, $\mathbf{y}_{cq}$ represents the channel c of the q-th observation image, $\mathbf{C}(\mathbf{s}_q)$ is the $N \times N$ warping matrix of motion vector $\mathbf{s}_q = [\theta_q, c_q, d_q]^t$, where θ_q is the rotation angle, and c_q and d_q are, respectively, the horizontal and vertical translations of the q-th observation image with respect to the reference frame, $\mathbf{x}_c$ represents the channel c we want to estimate. $\mathbf{y}_{cq}$ and $\mathbf{x}_c$ are both $N \times 1$ vectors.

We recover the fused image channels $\mathbf{x}_c$ by solving

$$\min \sum_{c\in\{R,G,B\}} L(\mathbf{x}_c) \quad \text{s.t.} \quad \mathbf{y}_{cq} = \mathbf{C}(\mathbf{s}_q)\mathbf{x}_c, \qquad \text{for } q = 1, \ldots, Q \text{ and } c \in \{R, G, B\}\,, \tag{2}$$

where

$$L(\mathbf{x}_c) = \mathbf{Q}(\mathbf{x}_c)\,, \tag{3}$$

with $\mathbf{Q}(\mathbf{x}_c)$ being the regularisation term proposed in [Saafin et al., 2015a, Saafin et al., 2015b] given by

$$\mathbf{Q}(\mathbf{x}_c) = \sum_{d\in\Delta}\sum_{i=1}^{N} \log_\epsilon(|\omega_d^{\mathbf{x}_c}(i)|)\,, \tag{4}$$

where

$$\log_\epsilon(|\omega_d^{\mathbf{x}_c}(i)|) = \begin{cases} \log(|\omega_d^{\mathbf{x}_c}(i)|), & |\omega_d^{\mathbf{x}_c}(i)| \geq \epsilon \\ \frac{|\omega_d^{\mathbf{x}_c}(i)|^2}{2\epsilon^2} - (\frac{1}{2} - \log(\epsilon)), & |\omega_d^{\mathbf{x}_c}(i)| \leq \epsilon \end{cases} \tag{5}$$

and $\omega_d^{\mathbf{x}_c}(i)$ is the i-th pixel of the filtered channel, that is,

$$\boldsymbol{\omega}_d^{\mathbf{x}_c} = \mathbf{F}_d\mathbf{x}_c\,, \tag{6}$$

where $\mathbf{F}_d$ is a high-pass filter operator, and the index $d \in \Delta$ denotes one of the filters in Δ. In this paper we use $\Delta = \{h, v, hv, vh\}$, where h, v represent respectively the first order horizontal and vertical difference filters, hv and vh the first order differences along diagonals.

3. RECONSTRUCTION APPROACH

Next we describe the optimisation approach to estimate the two main unknowns: the image $\mathbf{x}$ and the registration parameters $\mathbf{s}$. To convert the constrained optimisation problem in (2) into an unconstrained one utilising the alternating direction method of multipliers (ADMM), we define the following augmented Lagrangian functional

$$L(\mathbf{x}, \mathbf{s}, \boldsymbol{\lambda}) = \sum_{c\in\{R,G,B\}} L_c(\mathbf{x}_c, \mathbf{s}, \boldsymbol{\lambda}_c), \tag{7}$$

where

$$L_c(\mathbf{x}_c, \mathbf{s}, \boldsymbol{\lambda}_c) = \alpha L(\mathbf{x}_c) + \sum_{q=1}^{Q} \boldsymbol{\lambda}_{cq}^t(\mathbf{C}(\mathbf{s}_q)\mathbf{x}_c - \mathbf{y}_{cq}) + \frac{\beta}{2}\sum_{q=1}^{Q} \parallel \mathbf{C}(\mathbf{s}_q)\mathbf{x}_c - \mathbf{y}_{cq} \parallel^2, \tag{8}$$

and $L(\mathbf{x}_c)$ has been defined in (3), $\mathbf{s} = (\mathbf{s}_1, \ldots, \mathbf{s}_Q)$ is the set of motion vectors, $\boldsymbol{\lambda}_c = (\boldsymbol{\lambda}_{c1}, \ldots, \boldsymbol{\lambda}_{cQ})$ is the set of $N \times 1$ Lagrangian multiplier vectors $\boldsymbol{\lambda}_{cq}$, α and β are positive parameters, and $\parallel . \parallel$ denotes Euclidean norm. The ADMM leads to the following sequence of iterative unconstrained problems,

$$\mathbf{x}_c^{k+1} = \arg\min_{\mathbf{x}_c} L_c(\mathbf{x}_c, \mathbf{s}^k, \boldsymbol{\lambda}_c^k)\,, \tag{9}$$

$$\mathbf{s}^{k+1} = \arg\min_{\mathbf{s}} \sum_{c\in\{R,G,B\}} L_c(\mathbf{x}_c^{k+1}, \mathbf{s}, \boldsymbol{\lambda}_c^k)\,, \tag{10}$$

$$\boldsymbol{\lambda}_{cq}^{k+1} = \boldsymbol{\lambda}_{cq}^k - \beta[\mathbf{C}(\mathbf{s}_q^{k+1})\mathbf{x}_c^{k+1} - \mathbf{y}_{cq}]\,, \qquad q = 1, \ldots, Q, \tag{11}$$

where k is the iteration index. Notice that according to the ADMM formulation, $\mathbf{C}(\mathbf{s}_q)$ in (2) should not depend on the iteration index, as is not the case here. However, we have not encountered any convergence issues with this iterative procedure.

The first step is to optimise for the fused image $\mathbf{x}$ by combining (9) with (8), maximising-minimising the regularisation term $\mathbf{Q}(\mathbf{x}_c)$ in (4) for each colour component, we obtain the following update equation for $\mathbf{x}_c$ [Saafin et al., 2016],

$$\mathbf{x}_c^{k+1} = \left[\beta \sum_q \mathbf{C}^{k^t}(\mathbf{s}_q^k)\mathbf{C}^k(\mathbf{s}_q^k) + \alpha \sum_{d\in\Delta} \mathbf{F}_d^t \mathbf{\Omega}_{cd}^k \mathbf{F}_d\right]^{-1} \times \sum_q \mathbf{C}^k(\mathbf{s}_q^k)^t \left[\beta \mathbf{y}_{cq} - \lambda_{cq}^k\right], \tag{12}$$

where

$$\Omega_{cd}^k(i,i) = \min(1/|\omega_d^{\mathbf{x}_c^k}(i)|^2, 1/\epsilon^2). \tag{13}$$

The second step is to calculate the registration parameters using the estimated image $\mathbf{x}$. The approach we follow in this work is to simultaneously include all colour channels in the estimation procedure using the following equation

$$\mathbf{s}_q^{k+1} = \arg\min_{\mathbf{s}_q} \frac{\beta'}{2} \parallel \mathbf{C}(\mathbf{s}_q)\mathbf{z}_{\mathbf{x}^{k+1}} - \mathbf{z}_{\mathbf{y}_q} \parallel^2 . \tag{14}$$

where β' is a positive parameter, and $\mathbf{z}_\mathbf{x} = Y(\mathbf{x})$ where $Y(\mathbf{x})$ is calculated using

$$Y(\mathbf{x}) = 0.2989\,\mathbf{x}_R + 0.5870\,\mathbf{x}_G + 0.1140\,\mathbf{x}_B, \tag{15}$$

where $\mathbf{x}_R, \mathbf{x}_G$, and $\mathbf{x}_B$ are the R, G, and B channels of $\mathbf{x}$. $\mathbf{C}(\mathbf{s}_q)\mathbf{z}_\mathbf{x}$, can be approximated by expanding it into its first-order Taylor series around the previous value $\mathbf{s}_q^k$. We thus obtain (see [He et al., 2007])

$$\mathbf{C}(\mathbf{s}_q)\mathbf{z}_{\mathbf{x}^{k+1}} \approx \mathbf{C}(\mathbf{s}_q^k)\mathbf{z}_{\mathbf{x}^{k+1}} + \left[\mathbf{N}_1(\mathbf{s}_q^k)\mathbf{z}_{\mathbf{x}^{k+1}}, \mathbf{N}_2(\mathbf{s}_q^k)\mathbf{z}_{\mathbf{x}^{k+1}}, \mathbf{N}_3(\mathbf{s}_q^k)\mathbf{z}_{\mathbf{x}^{k+1}}\right] \times (\mathbf{s}_q - \mathbf{s}_q^k), \tag{16}$$

where $\mathbf{N}_i(\mathbf{s}_q^k)\mathbf{z}_{\mathbf{x}^{k+1}}$ is defined as

$$\left[\mathbf{N}_1(\mathbf{s}_q^k)\mathbf{z}_\mathbf{x}^{k+1}, \mathbf{N}_2(\mathbf{s}_q^k)\mathbf{z}_\mathbf{x}^{k+1}, \mathbf{N}_3(\mathbf{s}_q^k)\mathbf{z}_\mathbf{x}^{k+1}\right] = \left[(\mathbf{P}_1(\mathbf{s}_q^k)\mathbf{M}_1(\mathbf{s}_q^k) + \mathbf{P}_2(\mathbf{s}_q^k)\mathbf{M}_2(\mathbf{s}_q^k), \mathbf{M}_1(\mathbf{s}_q^k), \mathbf{M}_2(\mathbf{s}_q^k)\right] \tag{17}$$

and

$$\mathbf{M}_1(\mathbf{s}_q^k) = (\mathbf{I} - \mathbf{D}_{\mathbf{b}_q(\mathbf{s}_q)})(\mathbf{L}_{tr(\mathbf{s}_q)} - \mathbf{L}_{tl(\mathbf{s}_q)}) + \mathbf{D}_{\mathbf{b}_q(\mathbf{s}_q)}(\mathbf{L}_{br(\mathbf{s}_q)} - \mathbf{L}_{bl(\mathbf{s}_q)}) \tag{18}$$

$$\mathbf{M}_2(\mathbf{s}_q^k) = (\mathbf{I} - \mathbf{D}_{\mathbf{a}_q(\mathbf{s}_q)})(\mathbf{L}_{bl(\mathbf{s}_q)} - \mathbf{L}_{tl(\mathbf{s}_q)}) + \mathbf{D}_{\mathbf{a}_q(\mathbf{s}_q)}(\mathbf{L}_{br(\mathbf{s}_q)} - \mathbf{L}_{tr(\mathbf{s}_q)}) \tag{19}$$

$$\mathbf{P}_1(\mathbf{s}_q^k) = -[\mathbf{D}_\mathbf{u}\sin(\theta_q^k) + \mathbf{D}_\mathbf{v}\cos(\theta_q^k)] \tag{20}$$

$$\mathbf{P}_2(\mathbf{s}_q^k) = [\mathbf{D}_\mathbf{u}\cos(\theta_q^k) - \mathbf{D}_\mathbf{v}\sin(\theta_q^k)]. \tag{21}$$

where $\mathbf{I}$ is the identity matrix. $\mathbf{D}_{\mathbf{a}_q(\mathbf{s}_q)}$ and $\mathbf{D}_{\mathbf{b}_q(\mathbf{s}_q)}$ denote diagonal matrices with vectors $\mathbf{a}_q(\mathbf{s}_q)$ and $\mathbf{b}_q(\mathbf{s}_q)$ respectively in their diagonals which represent the horizontal and vertical displacements of observation q. $\mathbf{D}_\mathbf{u}$ and $\mathbf{D}_\mathbf{v}$ are diagonal matrices whose diagonals are vectors $\mathbf{u}$ and $\mathbf{v}$ respectively, representing pixel coordinates in $\mathbf{x}$. Matrices L_κ with $\kappa \in \{\mathbf{bl}(\mathbf{s}_q), \mathbf{br}(\mathbf{s}_q), \mathbf{tl}(\mathbf{s}_q), \mathbf{tr}(\mathbf{s}_q)\}$ are constructed in such a way that the product $L_\kappa\mathbf{z}$ produces pixels at the bottom-left, bottom-right, top-left, and top-right, locations of (u_q, v_q), respectively. Combining (16) with (14) and solving gives the update equation which we followed in our solution

$$\mathbf{s}_q^{k+1} = \mathbf{s}_q^k + \left[\lambda_q^k\right]^{-1} \Upsilon_q^k, \tag{22}$$

where λ_q^k and Υ_q^k correspond to the $q-$th observation at the $k-$th iteration with respectively $(i,j) \in \{1,2,3\}$ element and $i \in \{1,2,3\}$ element given by

$$\lambda_{qij}^k = \left[\mathbf{N}_i(\mathbf{s}_q^k)\mathbf{z}_{\mathbf{x}^{k+1}}\right]^t \mathbf{N}_j(\mathbf{s}_q^k)\mathbf{z}_{\mathbf{x}^{k+1}}, \tag{23}$$

$$\Upsilon_{qi}^k = \left[\mathbf{N}_i(\mathbf{s}_q^k)\mathbf{z}_{\mathbf{x}^{k+1}}\right]^t (\mathbf{z}_{\mathbf{y}_q} - \mathbf{N}_i(\mathbf{s}_q^k)\mathbf{z}_{\mathbf{x}^{k+1}}). \tag{24}$$

Utilising the estimated $\mathbf{s}_q^{k+1}$, the warping matrix can be calculated by [He et al., 2007, AlSaafin et al., 2016]

$$\begin{aligned}\mathbf{C}(\mathbf{s}_q)\mathbf{x} \approx\ & \mathbf{D}_{b_q(\mathbf{s}_q)}(\mathbf{I} - \mathbf{D}_{a_q(\mathbf{s}_q)})\mathbf{L}_{\mathbf{bl}(\mathbf{s}_q)}\mathbf{x} + (\mathbf{I} - \mathbf{D}_{b_q(\mathbf{s}_q)})\mathbf{D}_{a_q(\mathbf{s}_q)}\mathbf{L}_{\mathbf{tr}(\mathbf{s}_q)}\mathbf{x} \\ & + (\mathbf{I} - \mathbf{D}_{b_q(\mathbf{s}_q)})(\mathbf{I} - \mathbf{D}_{a_q(\mathbf{s}_q)})\mathbf{L}_{\mathbf{tl}(\mathbf{s}_q)}\mathbf{x} + \mathbf{D}_{b_q(\mathbf{s}_q)}\mathbf{D}_{a_q(\mathbf{s}_q)}\mathbf{L}_{\mathbf{br}(\mathbf{s}_q)}\mathbf{x}\,.\end{aligned} \tag{25}$$

The above approach for registering the observations assumes observations of the same sample, which is one application of the proposed algorithm. In cases where the observations are for the same tissue but with differences due to different staining the minimisation will look for the minimal distance between an observation and the estimated image, and hence the edges are not expected to colocalise but still optimal registration is obtained. The complete proposed algorithm is presented in Algorithm 1.

Algorithm 1 Proposed Image Fusion Algorithm

Require: Values α, β
Initialise $\mathbf{s}^0$, $\boldsymbol{\lambda}^0$, $\boldsymbol{\Omega}^0 = \{\boldsymbol{\Omega}_d^0, d \in \Delta\}$
$k = 0$
while convergence criterion is not met **do**
1. for $c \in \{R, G, B\}$
i Calculate $\mathbf{x}_c^{k+1}$ by solving (12).
ii For $d \in \Delta$, calculate $\boldsymbol{\Omega}_{cd}^{k+1}$ using (13).
iv For $q = 1, \ldots, Q$, update $\boldsymbol{\lambda}_{cq}^{k+1}$ using (11).
2. For $q = 1, \ldots, Q$, calculate $\mathbf{s}_q^{k+1}$ using (22).
3. Set $k = k + 1$
end while
return $\mathbf{x} = \left[\mathbf{x}_R^k, \mathbf{x}_G^k, \mathbf{x}_B^k\right]$.

4. EXPERIMENTS

We used DP images to perform two main experiments on normalised images. In the first experiment we used simulated DP observation images to mathematically assess the quality of the output image. The second experiment used real DP images. For both experiments, the stopping criteria are either a maximum number of iterations (25) or

$$\frac{\| \mathbf{x}^{k+1} - \mathbf{x}^k \|}{\| \mathbf{x}^k \|} \leq 10^{-3}\,. \tag{26}$$

In the first experiment, to simulate the observation images, we started with the image shown in Figure 1(a) referred later as the original image. It is for a tissue stained with haematoxylin and eosin and it is available on internet. Four images were generated from the original; each by performing a random warping of three parameters including horizontal, vertical and rotational displacements. Figures 1(b,c) show two of the four synthesised images which were fed to the proposed algorithm to find an estimate of the original image. The fused image is shown in Figure 1(d). To compare the estimated image with the original we use the peak signal to noise ratio (PSNR) measure for colour RGB images is calculated as

$$PSNR = 10\log(\frac{3N \cdot \max^2(\mathbf{x})}{\| \hat{\mathbf{x}} - \mathbf{x} \|^2})\,, \tag{27}$$

where $\max(\mathbf{x})$ represents the maximum possible value in $\mathbf{x}$, and N is the number of pixels $\mathbf{x}$. In the performed experiment the obtained PSNR was 45.09 dB. The number of iterations required to obtain the shown result was 8. The same experiment was performed for the original image shown in Figure 1(e) and the fused image is shown in Figure 1(h) giving PSNR=41.69 dB after performing 25 iterations. In both experiments the number of observations was 4 (although only two of them were shown in Figure 1).

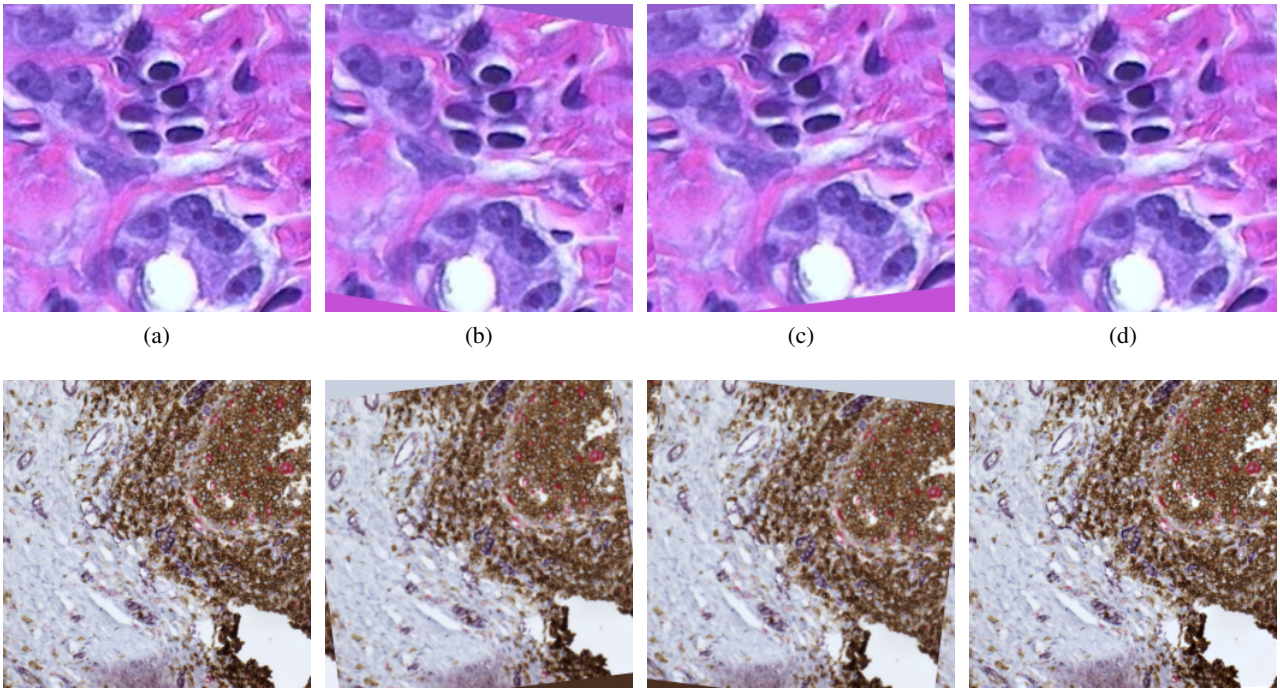

Fig. 1: Image fusion of simulated unregistered DP images. (a) original image, (b,c) 2 of 4 observations, (d) estimated image with PSNR=45.09 dB (e) original image, (f,g) 2 of 4 observations, (h) estimated image with PSNR=41.69 dB.

In the second experiment we used five images acquired during a sequential staining experiment for the breast tissue samples shown in Figure 2 of human epidermal growth factor receptor 2 (a), haematoxylin-eosin (b), estrogen receptor (c), Ki67 (d), and progesterone receptor (e) sections [Déniz et al., 2015]. The real observations were fused into the image shown in Figure 2(f). The visualisation and contrast of the estimated image can be further enhanced using a histogram stretching operation as shown in Figure 2(g).

The high PSNR and the visual assessment of the output images in both experiments prove the excellent performance of our proposed algorithm.

5. CONCLUSIONS

Colour digital pathology images can be fused to combine information from different images of a sample. This can help in better visualising abnormalities, diagnosing the stage of a disease and observing the development of illness. Besides, the fused image can be analysed instead of analysing multiple images. This is important for automatic analysis where it is difficult to analyse multiple images at the same time. Accurate estimation of DP image registration parameters which is challenging but vital for diagnosis tasks has been achieved at high convergence rates. Similar application can benefit from this proposal to enhance diagnostics, analysis, and historical documentation. Future work will aim at extending this proposed work to remove the blur which is expected in DP images due to unfocussed regions that appear as a result of the three dimensional structure of a scanned slide.

Acknowledgement

This work was supported by the EC under Marie Curie grant actions, grant No. 612471, Academia and Industry Collaboration for Digital Pathology (AIDPATH) project (`http://aidpath.eu/`).

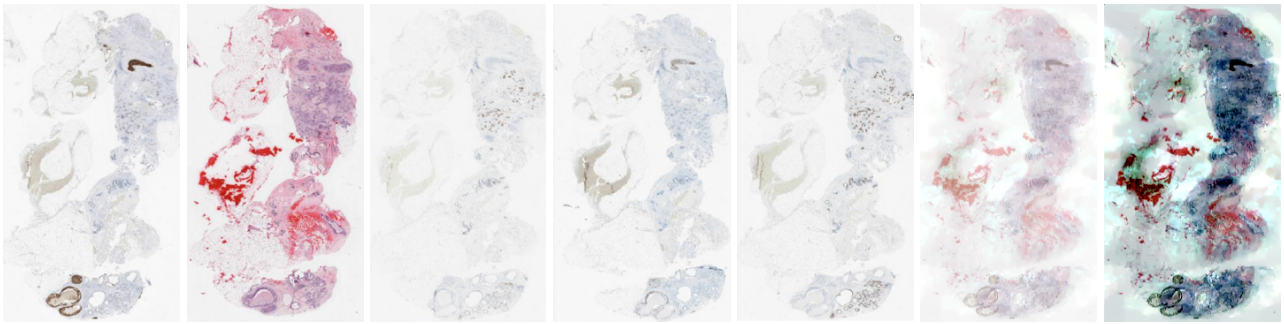

(a) (b) (c) (d) (e) (f) (g)

Fig. 2: Image fusion of unregistered sequentially stained real images of breast tissue WSI. (a) human epidermal growth factor receptor 2, (b) haematoxylin-eosin, (c) estrogen receptor, (d) Ki67 protein, (e) progesterone receptor, (f) estimated image, (g) estimated image after histogram stretching.

6. REFERENCES

[AlSaafin et al., 2016] AlSaafin, W., Villena, S., Vega, M., Molina, R., and Katsaggelos, A. K. (2016). Compressive sensing super resolution from multiple observations with application to passive millimeter wave images. *Digital Signal Processing*, 50:180–190.

[Chajari et al., 2002] Chajari, M., Lacroix, J., Peny, A., Chesnay, E., Batalla, A., Henry-Amar, M., Delcambre, C., Génot, J., Fruchard, C., and Bardet, S. (2002). Gallium-67 scintigraphy in lymphoma: is there a benefit of image fusion with computed tomography? *European Journal of Nuclear Medicine and Molecular Imaging*, 29(3):380.

[Déniz et al., 2015] Déniz, O., Toomey, D., Conway, C., and Bueno, G. (2015). Multi-stained whole slide image alignment in digital pathology. In *SPIE Medical Imaging*, pages 94200Z–94200Z.

[Galande and Patil, 2013] Galande, A. and Patil, R. (2013). The art of medical image fusion: A survey. In *International Conference on Advances in Computing, Communications and Informatics (ICACCI)*, pages 400–405.

[Glatz-Krieger et al., 2006] Glatz-Krieger, K., Spornitz, U., Spatz, A., Mihatsch, M. J., and Glatz, D. (2006). Factors to keep in mind when introducing virtual microscopy. *Virchows Archiv*, 448(3):248–255.

[Gooding et al., 2010] Gooding, M., Rajpoot, K., Mitchell, S., Chamberlain, P., Kennedy, S., and Noble, J. (2010). Investigation into the fusion of multiple 4-d fetal echocardiography images to improve image quality. *Ultrasound in Medicine & Biology*, 36(6):957–966.

[Hamilton et al., 2014] Hamilton, P. W., Bankhead, P., Wang, Y., Hutchinson, R., Kieran, D., McArt, D. G., James, J., and Salto-Tellez, M. (2014). Digital pathology and image analysis in tissue biomarker research. *Methods*, 70(1):59–73.

[He et al., 2007] He, Y., Yap, K., Chen, L., and Chau, L.-P. (2007). A nonlinear least square technique for simultaneous image registration and super-resolution. *IEEE Transactions on Image Processing*, 16(11):2830–2841.

[Holupka et al., 1998] Holupka, E., Kaplan, I., and Burdette, E. (1998). Ultrasound localization and image fusion for the treatment of prostate cancer. US Patent 5,810,007.

[Irshad et al., 2014] Irshad, H., Veillard, A., Roux, L., and Racoceanu, D. (2014). Methods for nuclei detection, segmentation, and classification in digital histopathology: A review. *IEEE Reviews in Biomedical Engineering*, 7:97–114.

[James and Dasarathy, 2014] James, A. and Dasarathy, B. (2014). Medical image fusion: A survey of the state of the art. *Information Fusion*, 19:4–19.

[Kobayashi et al., 2007] Kobayashi, H., Hama, Y., Koyama, Y., Barrett, T., Regino, C., Urano, Y., and Choyke, P. (2007). Simultaneous multicolor imaging of five different lymphatic basins using quantum dots. *Nano Letters*, 7(6):1711–1716.

[Kothari et al., 2013] Kothari, S., Phan, J. H., Stokes, T. H., and Wang, M. D. (2013). Pathology imaging informatics for quantitative analysis of whole-slide images. *Journal of the American Medical Informatics Association*, 20(6):1099–1108.

[Saafin and Schaefer, 2017] Saafin, W. and Schaefer, G. (2017). Pre-processing techniques for colour digital pathology image analysis. In *Annual Conference on Medical Image Understanding and Analysis*, pages 551–560.

[Saafin et al., 2015a] Saafin, W., Vega, M., Molina, R., and Katsaggelos, A. K. (2015a). Image super-resolution from compressed sensing observations. In *IEEE International Conference on Image Processing (ICIP)*, pages 4268–4272.

[Saafin et al., 2016] Saafin, W., Vega, M., Molina, R., and Katsaggelos, A. K. (2016). Compressed sensing super resolution of color images. In *24th European Signal Processing Conference (EUSIPCO)*, pages 1563–1567.

[Saafin et al., 2015b] Saafin, W., Villena, S., Vega, M., Molina, R., and Katsaggelos, A. K. (2015b). Pmmw image super resolution from compressed sensing observations. In *23rd European Signal Processing Conference (EUSIPCO)*, pages 1815–1819.

[Sonn et al., 2014] Sonn, G., Chang, E., Natarajan, S., Margolis, D., Macairan, M., Lieu, P., Huang, J., Dorey, F., Reiter, R., and Marks, L. (2014). Value of targeted prostate biopsy using magnetic resonance–ultrasound fusion in men with prior negative biopsy and elevated prostate-specific antigen. *European Urology*, 65(4):809–815.

[Townsend and Beyer, 2002] Townsend, D. W. and Beyer, T. (2002). A combined pet/ct scanner: the path to true image fusion. *The British Journal of Radiology*, 75(suppl_9):S24–S30.

[Veta et al., 2014] Veta, M., Pluim, J. P., van Diest, P. J., and Viergever, M. A. (2014). Breast cancer histopathology image analysis: A review. *IEEE Transactions on Biomedical Engineering*, 61(5):1400–1411.

[Wang et al., 2014] Wang, C., Ka, S., and Chen, A. (2014). Robust image registration of biological microscopic images. *Scientific Reports*, 4.

[Weinstein et al., 2009] Weinstein, R. S., Graham, A. R., Richter, L. C., Barker, G. P., Krupinski, E. A., Lopez, A. M., Erps, K. A., Bhattacharyya, A. K., Yagi, Y., and Gilbertson, J. R. (2009). Overview of telepathology, virtual microscopy, and whole slide imaging: prospects for the future. *Human Pathology*, 40(8):1057–1069.